Response of the Hadley Circulation to Convective Forcing in the ITCZ

JAMES J. HACK

National Center for Atmospheric Research, Boulder, Colorado*

WAYNE H. SCHUBERT AND DUANE E. STEVENS

Department of Atmospheric Science, Colorado State University, Fort Collins, Colorado

HUNG-CHI KUO

Naval Environmental Prediction Research Facility, Monterey, California

(Manuscript received 16 November 1988, in final form 5 April 1989)

ABSTRACT

Through the use of a zonal balance model we investigate the response of the mean meridional circulation to a specified diabatic forcing for both resting and nonresting zonal flows. The use of a potential latitude coordinate and transformed meridional circulation components results in a simplified meridional circulation equation in which the variable coefficients are the normalized potential vorticity and inertial stability. Solutions of this equation illustrate how latent heat release away from the equator forces a winter hemisphere Hadley cell that is more intense than the summer hemisphere cell. This asymmetric response is due primarily to the anisotropy associated with the spatial variation of the inertial stability field. Despite the sensitivity of the meridional circulation to the location and breadth of the forcing, the low latitude thermodynamic response is for the most part insensitive as long as the total latent heat release remains the same.

Numerical solutions of the zonal balance model result in evolving zonal wind and temperature fields that modify the potential vorticity and inertial stability fields. In the vicinity of the ITCZ, the potential vorticity becomes large in the lower troposphere and small in the upper troposphere which, in addition to modifying the response of the meridional circulation, generates the necessary dynamical conditions for wave instability. Since the inertial stability is only slightly modified, however, the basic anisotropy in the response of the meridional circulation remains. At the same time, the evolving zonal wind and temperature fields result in an increasing dynamic efficiency of latent heat release, which leads to an accelerated growth of zonal kinetic energy, especially when the ITCZ is located poleward of 10 degrees latitude.

1. Introduction

There appear to be two conceptual views of the Hadley circulation and the ITCZ. The first, often adopted in studies of the atmospheric general circulation and climate, considers the Hadley circulation and the ITCZ as monthly (or seasonally) and zonally averaged phenomena that can be simulated with thermally forced, frictionally controlled, steady state models. This is essentially the view adopted by Schneider and Lindzen (1977), Schneider (1977), Held and Hou (1980), and Lindzen and Hou (1988), who solve for steady circulations forced by convection and/or temperature deviations from a specified equilibrium temperature. The second view, often expressed in the context of tropical weather analysis and forecasting, is that the Hadley circulation and the ITCZ are phenomena that can be identified on individual weather maps and whose fluctuations can be followed day to day (hence the terms breakdown of the ITCZ, reformation of the ITCZ and trade wind surges). An example of such fluctuations is shown in Fig. 1, which consists of three GOES IR images from 1646 UTC on 26 July, 3 August and 12 August 1988. On 26 July an elongated east–west zone of convection covers the eastern Pacific at about 10°N. Eight days later (3 August) this ITCZ has broken down into a series of tropical cyclones. Nine days later (12 August) the ITCZ has reformed at about 10°N. It is this second view that we shall adopt here. In particular, we will study evolving circulations in a frictionless, thermally forced model. These solutions illuminate several interesting aspects of equatorial balanced dynamics.

Regardless of which conceptual view is adopted, one of the most interesting features of the Hadley circulation is the difference in the strengths of its two cells when the ITCZ is displaced off the equator. This can be illustrated by comparing the June–August and the December–February meridional circulation fields. In June, July and August most of the latent heat release

* The National Center for Atmospheric Research is sponsored by the National Science Foundation.

Corresponding author address: Dr. James J. Hack, National Center for Atmospheric Research, P.O. Box 3000, Boulder, CO 80307.

© 1989 American Meteorological Society

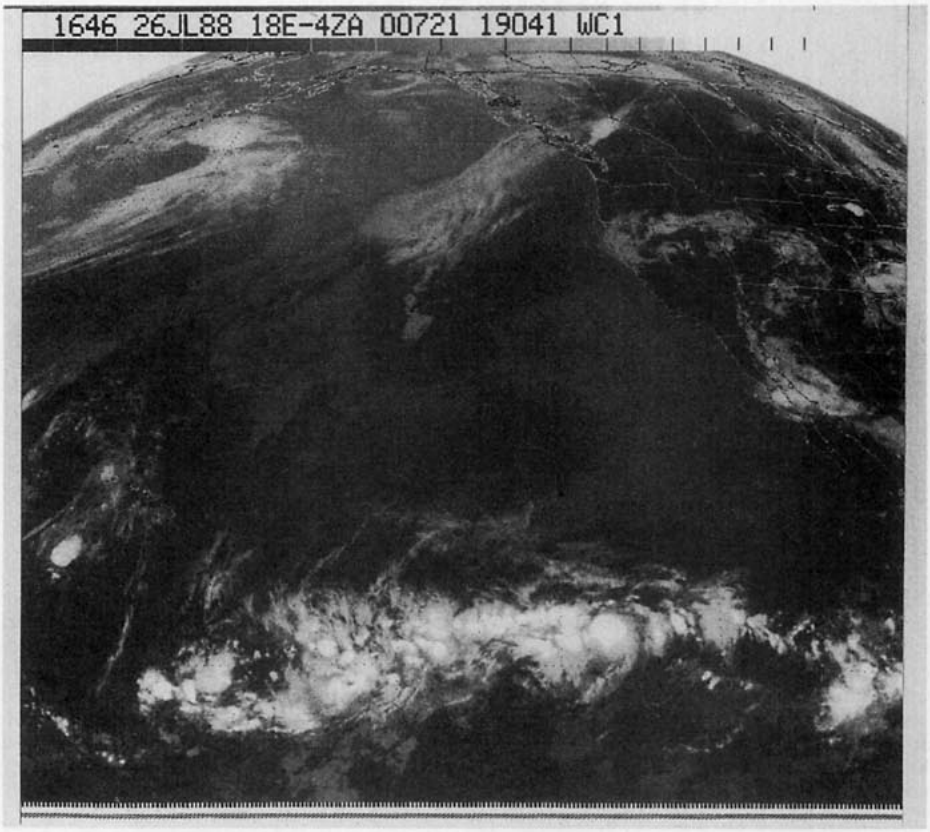

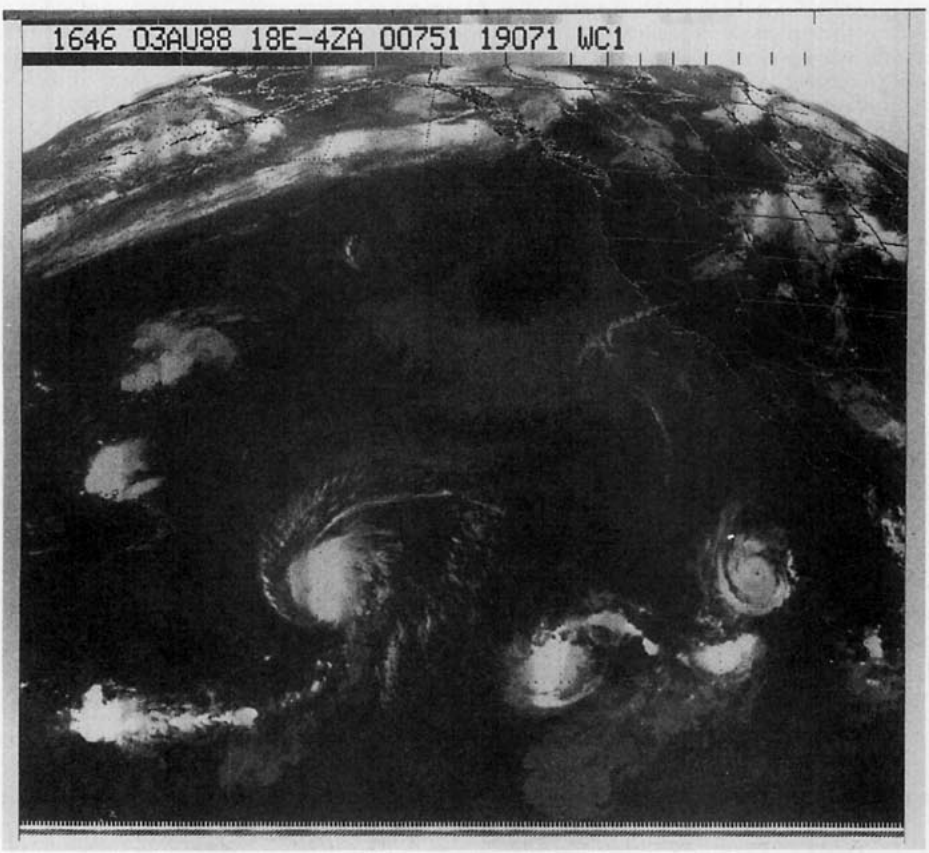

FIG. 1. GOES IR images at 1646 UTC on (a) 26 July, (b) 3 August, and (c) 12 August 1988. Note the breakdown and reformation of the ITCZ.

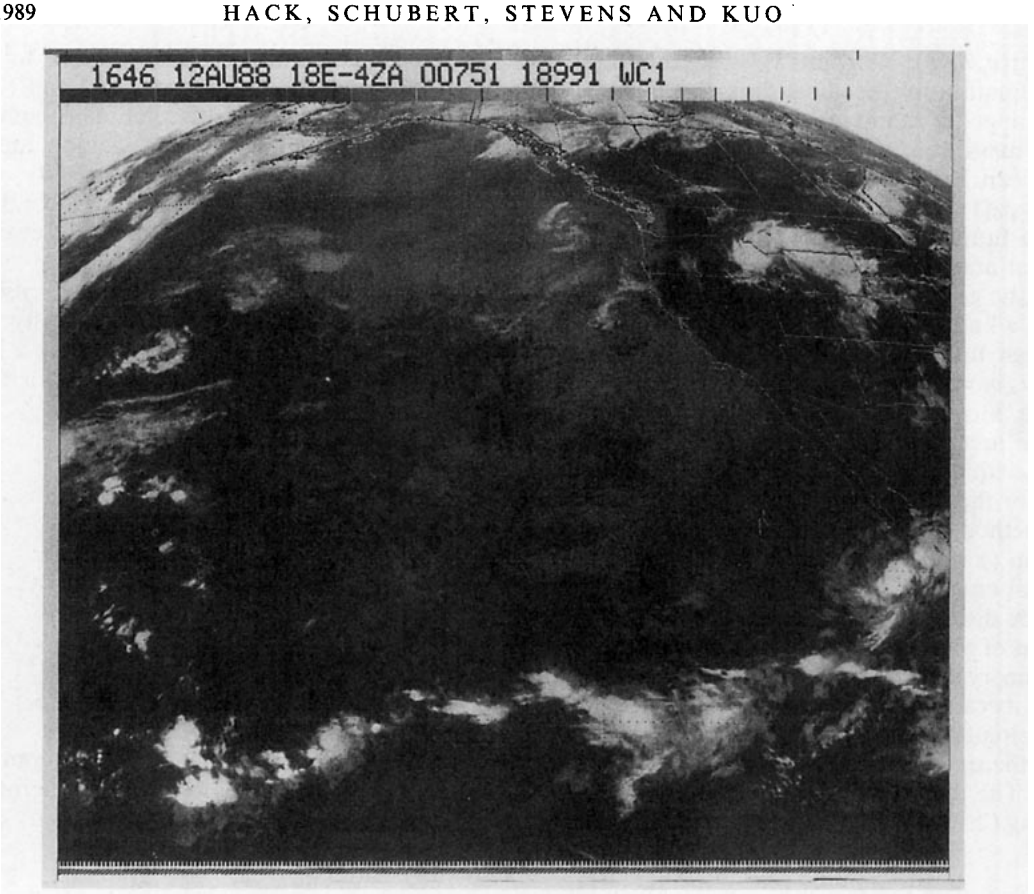

FIG. 1. (*Continued*)

associated with the ITCZ occurs north of the equator. The meridional circulation associated with this latent heat release exhibits a distinct preference for the winter hemisphere cell, i.e., the low level air which is drawn into the ascending region comes mostly from the south. In December, January and February most of the latent heat release occurs south of the equator, and the low level air is drawn into the ascending region primarily from the north. This effect is clearly illustrated in the observational analyses of Newell et al. (1972, Fig. 3.19) and Oort (1983, Fig. F-44); it has also been theoretically reproduced by Gill (1982, section 11.14) and by Lindzen and Hou (1988), who applied the simplified theory of Held and Hou (1980) to diabatic heating centered at a latitude off the equator.

This paper has three major goals. The first is to understand how the difference in mass flux between the two halves of the Hadley circulation depends on the latitude of the ITCZ convection and on the zonal flow in which the convection is imbedded. The second is to understand how the latitude of the ITCZ influences the efficiency with which zonal kinetic energy is produced. The third is to understand how ITCZ convection can produce zonal flows that are unstable to zonally asymmetric wave disturbances. We will use the nonsteady balanced system of equations to illustrate the atmospheric response to low latitude zonally symmetric diabatic heat sources with varying horizontal space scales. Our results involve the solution of a diagnostic meridional circulation equation which is formulated in an angular momentum coordinate we call the potential latitude. Solution of this equation requires knowledge of the potential vorticity, inertial stability, and diabatic heating fields. Since our approach to the problem neglects zonal asymmetries and frictional effects, it will not directly address the details of the longer term seasonal structure of the mean meridional circulation. Nevertheless, our results will clearly show that the difference in the strengths of the winter and summer Hadley cells is due primarily to the anisotropy associated with the spatial variation of the inertial stability field.

2. Governing equations

Our model of the Hadley circulation is based on the assumptions that all fields are independent of longitude and that the zonal flow is frictionless and balanced. Using the subscript zero to denote a reference value, the pseudo-height coordinate can be defined as $z = [1$

$-(p/p_0)^\kappa](c_p\theta_0/g)$. With this vertical coordinate the balance equation for the zonal flow, the approximate absolute angular momentum principle, hydrostatic balance, mass continuity and the thermodynamic equation can be written as (2.1)–(2.5) of Table 1, where $\rho = \rho_0[1-(gz/c_p\theta_0)]^{(1-\kappa)/\kappa}$ is the pseudo-density (a known function of z), u, v and w are the zonal, meridional and vertical components of the velocity, and G is the geopotential. The diabatic term Q is regarded as a known function of space and time.

Although the set (2.1)–(2.5) is closed in the unknowns u, v, w, θ and G, it is an inconvenient set for prediction. More suitable forms can be obtained in two ways. The first method involves replacing one of the prognostic equations, (2.2) or (2.5), with a diagnostic relation for the meridional circulation $(\rho v, \rho w)$. The second method involves elimination of the meridional circulation $(\rho v, \rho w)$ to obtain a second order partial differential equation for $\partial G/\partial t$. This second method will not be discussed here [see Schubert (1985) for a discussion of this method in the context of semigeostrophic theory]. To proceed with the first method we note that, because of the continuity equation, the meridional circulation components can be expressed in terms of the single streamfunction variable ψ as given in (2.6). The diagnostic equation for ψ is derived by combining (2.1) and (2.3) to obtain the thermal wind equation, and then using this equation to eliminate local time derivatives between (2.2) and (2.5). The result is the meridional circulation equation (2.7a) where the variable coefficients A, B and C are the static stability, baroclinity and inertial stability, which are defined in (2.7b–d). The boundary conditions for (2.7a) are simply homogeneous Dirichlet conditions on ψ.

Let us now discuss the potential vorticity principle associated with (2.1)–(2.5). The vorticity vector associated with the predictive component u lies in the (ϕ, z) plane. The governing equation for this vector vorticity takes the form

$$\rho \frac{D}{Dt}\left(\frac{\boldsymbol{\zeta}}{\rho}\right) = (\boldsymbol{\zeta}\cdot\nabla)\mathbf{v}, \tag{2.8}$$

where

$$\frac{D}{Dt} = \frac{\partial}{\partial t} + v\frac{\partial}{a\partial\phi} + w\frac{\partial}{\partial z}, \tag{2.9}$$

$$\boldsymbol{\zeta} = \left(\frac{\partial u}{\partial z}, 2\Omega\sin\phi - \frac{\partial(u\cos\phi)}{a\cos\phi\partial\phi}\right), \tag{2.10}$$

$\nabla = (\partial/a\partial\phi, \partial/\partial z)$ and $\mathbf{v} = (v, w)$. By combining the vector vorticity equation (2.8) with the thermodynamic equation, we obtain the potential vorticity equation

TABLE 1. Governing equations.

$$\left(2\Omega\sin\phi + \frac{u\tan\phi}{a}\right)u + \frac{\partial G}{a\partial\phi} = 0 \tag{2.1}$$

$$\frac{\partial u}{\partial t} + w\frac{\partial u}{\partial z} - \left(2\Omega\sin\phi - \frac{\partial(u\cos\phi)}{a\cos\phi\partial\phi}\right)v = 0 \tag{2.2}$$

$$\frac{\partial G}{\partial z} = \frac{g}{\theta_0}\theta \tag{2.3}$$

$$\frac{\partial(v\cos\phi)}{a\cos\phi\partial\phi} + \frac{\partial(\rho w)}{\rho\partial z} = 0 \tag{2.4}$$

$$\frac{\partial\theta}{\partial t} + v\frac{\partial\theta}{a\partial\phi} + w\frac{\partial\theta}{\partial z} = \frac{\theta}{c_pT}Q = \mathcal{Q} \tag{2.5}$$

$$(\rho v, \rho w) = \left(-\frac{\partial\psi}{\partial z}, \frac{\partial(\psi\cos\phi)}{a\cos\phi\partial\phi}\right) \tag{2.6}$$

$$\frac{\partial}{a\partial\phi}\left(A\frac{\partial(\psi\cos\phi)}{a\cos\phi\partial\phi} + B\frac{\partial\psi}{\partial z}\right) + \frac{\partial}{\partial z}\left(B\frac{\partial(\psi\cos\phi)}{a\cos\phi\partial\phi} + C\frac{\partial\psi}{\partial z}\right) = \frac{g}{\theta_0}\frac{\partial\mathcal{Q}}{a\partial\phi} \tag{2.7a}$$

$$A = \frac{g}{\rho\theta_0}\frac{\partial\theta}{\partial z}, \tag{2.7b}$$

$$B = -\frac{g}{\rho\theta_0}\frac{\partial\theta}{a\partial\phi} = \frac{\partial u}{\rho\partial z}\left(2\Omega\sin\phi + \frac{2u\tan\phi}{a}\right) \tag{2.7c}$$

$$C = \frac{\zeta}{\rho}\left(2\Omega\sin\phi + \frac{2u\tan\phi}{a}\right) \tag{2.7d}$$

$$2\Omega\sin\Phi\frac{\cos^2\Phi}{\cos^2\phi}u^* + \frac{\partial G^*}{a\partial\Phi} = 0 \tag{3.1}$$

$$\frac{\partial u^*}{\partial T} - 2\Omega v^*\sin\phi = 0 \tag{3.2}$$

$$\frac{\partial G^*}{\partial Z} = \frac{g}{\theta_0}\theta \tag{3.3}$$

$$\frac{\partial(v^*\cos\Phi)}{a\cos\Phi\partial\Phi} + \frac{\partial(\rho w^*)}{\rho\partial Z} = 0 \tag{3.4}$$

$$\frac{\partial\theta}{\partial T} + \frac{\theta_0}{g}q\rho w^* = \mathcal{Q} \tag{3.5}$$

$$(\rho v^*, \rho w^*) = \left(-\frac{\partial\psi^*}{\partial Z}, \frac{\partial(\psi^*\cos\Phi)}{a\cos\Phi\partial\Phi}\right) \tag{3.6}$$

$$\frac{\partial}{a\partial\Phi}\left(q\frac{\partial(\psi^*\cos\Phi)}{a\cos\Phi\partial\Phi}\right) + \frac{\partial}{\partial Z}\left(s\frac{\partial\psi^*}{\partial Z}\right) = \frac{g}{\theta_0}\frac{\partial\mathcal{Q}}{a\partial\Phi} \tag{3.7a}$$

$$q = \frac{g}{\rho\theta_0}\frac{\zeta}{2\Omega\sin\Phi}\frac{\partial\theta}{\partial Z} \tag{3.7b}$$

$$s = \frac{4\Omega^2}{\rho}\sin\phi\sin\Phi\frac{\cos^4\Phi}{\cos^4\phi} \tag{3.7c}$$

$$\rho \frac{DP}{Dt} = \boldsymbol{\zeta} \cdot \nabla Q, \tag{2.11}$$

where

$$P = \frac{1}{\rho} \boldsymbol{\zeta} \cdot \nabla \theta \tag{2.12}$$

is the Rossby–Ertel potential vorticity.

3. Potential latitude coordinate transformation

We shall now transform Eqs. (2.1)–(2.7) into Eqs. (3.1)–(3.7) of Table 1. To do this we introduce the potential latitude Φ, which is related to the latitude ϕ and the zonal wind u by

$$\sin\Phi = \sin\phi - \frac{u\cos\phi}{a\Omega(\sin\Phi + \sin\phi)}, \tag{3.8a}$$

which can be rearranged to yield

$$\Omega a \cos^2\Phi = \Omega a \cos^2\phi + u\cos\phi. \tag{3.8b}$$

Since the right-hand side of (3.8b) is the absolute angular momentum per unit mass, the potential latitude can be interpreted as the latitude to which an air parcel must be moved (conserving absolute angular momentum) in order for its zonal wind component to vanish. Even when the absolute angular momentum is not conserved, we might expect certain advantages in using it as a coordinate in place of ϕ. This has been discussed by Shutts (1980). Here we follow this general approach but use as the new coordinate the potential latitude Φ. To insure that the transformation (3.8a) exists, we limit ourselves to flows in which $u\cos\phi \leqslant \Omega\, a \sin^2\phi$. The use of the potential latitude coordinate in the present zonal balance model is analogous to the use of the potential radius coordinate in the Eliassen balanced vortex model of tropical cyclones (Schubert and Hack 1983; Hack and Schubert 1986; Schubert and Alworth 1987). Thus, let us consider (Φ, Z, T) space, where $Z = z$ and $T = t$. The symbols Z and T are introduced to distinguish partial derivatives at fixed ϕ ($\partial/\partial z$ and $\partial/\partial t$) from partial derivatives at fixed Φ ($\partial/\partial Z$ and $\partial/\partial T$). Derivatives in (ϕ, z, t) space are then related to derivatives in (Φ, Z, T) space by

$$\frac{\partial}{\partial t} = \frac{\partial\Phi}{\partial t}\frac{\partial}{\partial\Phi} + \frac{\partial}{\partial T}, \tag{3.9}$$

$$\frac{\partial}{\partial\phi} = \frac{\partial\Phi}{\partial\phi}\frac{\partial}{\partial\Phi}, \tag{3.10}$$

$$\frac{\partial}{\partial z} = \frac{\partial\Phi}{\partial z}\frac{\partial}{\partial\Phi} + \frac{\partial}{\partial Z}. \tag{3.11}$$

Another way of writing (3.10) is

$$\frac{\partial}{\cos\phi\partial\phi} = \left(\frac{\zeta}{2\Omega\sin\Phi}\right)\frac{\partial}{\cos\Phi\partial\Phi}, \tag{3.12}$$

where ζ is the vertical component of the absolute vorticity vector defined in (2.10). Thus, in regions where $\zeta > 2\Omega\sin\Phi$, the Φ coordinate provides a natural stretching which is analogous to the way the geostrophic coordinate provides stretching around fronts in semigeostrophic theory (Hoskins and Bretherton 1972).

Using (3.11), (3.12) and (3.8) we can show that

$$\boldsymbol{\zeta}\cdot\nabla = \frac{\partial u}{\partial z}\frac{\partial}{a\partial\phi} + \zeta\frac{\partial}{\partial z} = \zeta\frac{\partial}{\partial Z}, \tag{3.13}$$

which allows the Rossby–Ertel potential vorticity (2.12) to be expressed in the more compact form

$$P = \frac{\zeta}{\rho}\frac{\partial\theta}{\partial Z}. \tag{3.14}$$

From (3.9)–(3.11) we can also easily show that the total derivative can be written as

$$\frac{D}{Dt} = \frac{\partial}{\partial T} + w\frac{\partial}{\partial Z}, \tag{3.15}$$

which should be compared to (2.9).

Let us now introduce the transformed velocity components u^*, v^*, w^* and the potential function G^* defined by

$$u^* = \left(\frac{\cos\phi}{\cos\Phi}\right)u, \tag{3.16}$$

$$v^* = \left(\frac{\cos\phi}{\cos\Phi}\right)\left(v - wa\frac{\partial\phi}{\partial Z}\right), \tag{3.17}$$

$$w^* = \left(\frac{2\Omega\sin\Phi}{\zeta}\right)w, \tag{3.18}$$

$$G^* = G + \tfrac{1}{2}u^2. \tag{3.19}$$

Using (2.10), (3.12) and (3.16) it can be shown that

$$\left(2\Omega\sin\phi - \frac{\partial(u\cos\phi)}{a\cos\phi\partial\phi}\right)\Big/(2\Omega\sin\phi)$$
$$= (2\Omega\sin\Phi)\Big/\left(2\Omega\sin\Phi + \frac{\partial(u^*\cos\Phi)}{a\cos\Phi\partial\Phi}\right), \tag{3.20}$$

which means that as $-\partial(u^*\cos\Phi)/(a\cos\Phi\partial\Phi)$ approaches $2\Omega\sin\Phi$, the vertical component of absolute vorticity becomes much larger than the local Coriolis parameter. This is analogous to what happens when using geostrophic coordinates in semigeostrophic theory (Hoskins 1975) and when using the potential radius coordinate in the Eliassen balanced vortex model of tropical cyclones (Schubert and Hack 1983). In a further analogy with semigeostrophic theory the application of (3.9)–(3.11) to (3.19) leads to

$$\frac{\partial G}{\partial t} = \frac{\partial G^*}{\partial T}, \tag{3.21}$$

$$\frac{\partial G}{\cos\phi\,\partial\phi} = \left(\frac{2\Omega\sin\phi + (u\tan\phi)/a}{2\Omega\sin\Phi}\right)\frac{\partial G^*}{\cos\Phi\partial\Phi}, \tag{3.22}$$

$$\frac{\partial G}{\partial z} = \frac{\partial G^*}{\partial Z}. \tag{3.23}$$

The use of (3.8)–(3.23) allows us to transform (2.1)–(2.5) to (3.1)–(3.5) of Table 1. Some details of this transformation are given in appendix A. In comparing the two columns of Table 1, we note that (3.1)–(3.5) represent a simplification over (2.1)–(2.5) since the mathematical forms of the hydrostatic and continuity equations have remained essentially unchanged while the balance, zonal momentum and thermodynamic equations have all been simplified. The derivation of (3.7) proceeds in a fashion similar to the derivation of (2.7), i.e., the transformed thermal wind balance is used to eliminate the time derivative terms between (3.2) and (3.5). The lack of terms involving w^* in (3.2) and v^* in (3.5) leads to a meridional circulation equation (3.7) which has no cross-derivative terms. Since the variable coefficient q is proportional to $P/(2\Omega\sin\Phi)$, we will refer to it as the normalized potential vorticity. Note that q plays the role of static stability in (3.5). When the zonal flow vanishes everywhere, $\sin\Phi = \sin\phi$ and (3.7b) reduces to $\rho q = (g/\theta_0)\partial\theta/\partial z$, the square of the Brunt–Väisälä frequency.

There are two interesting connections between the transverse circulation equations (2.7) and (3.7). First, using (2.7b–d), (3.7b–c) and (3.14) we can show that $(AC - B^2)\cos^2\phi\cos^2\Phi = qs\cos^4\phi = g/(\rho\theta_0)P2\Omega \times \sin\phi\cos^4\Phi$, so that ellipticity in the transverse circulation problem can be judged by whether $(AC - B^2) > 0$, $qs > 0$ or $P\sin\phi > 0$. Later (Fig. 8) we shall see that when an ITCZ develops off the equator in the Northern Hemisphere, Southern Hemispheric air with negative P is drawn into the Northern Hemisphere at low levels and Northern Hemispheric air with positive P is pushed into the Southern Hemisphere at high levels. This results in small regions near the equator where the transverse circulation equations (2.7) and (3.7) become nonelliptic. For a discussion of the relation of ellipticity to symmetric instability near the equator, see Stevens (1983). The second connection between (2.7) and (3.7) is established by using (2.6), (3.6), (3.11) and (3.16) to show that $\psi^*\cos\Phi = \psi\cos\phi$. Thus, isolines of $\psi^*\cos\Phi$ drawn in the (Φ, Z) plane give the meridional flux $(\rho v^*\cos\Phi, \rho w^*\cos\Phi)$ while the same isolines drawn in the (ϕ, z) plane give the meridional flux $(\rho v\cos\phi, \rho w\cos\phi)$.

4. Energetics and efficiency

Before we proceed to obtain solutions of the equations in Table 1, let us briefly discuss the energy principles associated with these equations. From the original system (2.1)–(2.5) we can derive the following potential and kinetic energy equations

$$\frac{d\mathcal{P}}{dt} = \mathscr{H} - \mathscr{C}, \tag{4.1}$$

$$\frac{d\mathcal{K}}{dt} = \mathscr{C}, \tag{4.2}$$

where

$$\mathcal{P} = \int\int c_p T\rho a\cos\phi d\phi dz, \tag{4.3}$$

$$\mathcal{K} = \int\int \tfrac{1}{2}u^2\rho a\cos\phi d\phi dz, \tag{4.4}$$

$$\mathscr{H} = \int\int Q\rho a\cos\phi d\phi dz, \tag{4.5}$$

$$\mathscr{C} = \int\int \frac{g}{\theta_0} w\theta\rho a\cos\phi d\phi dz. \tag{4.6}$$

The integrals in (4.3)–(4.6) extend from the South Pole to the North Pole and from $z = 0$ to z_T. Thus, $\mathcal{P}$ and $\mathcal{K}$ denote the total potential and kinetic energies of the atmosphere, $\mathscr{H}$ the total heating, and $\mathscr{C}$ the rate of conversion of total potential energy into kinetic energy.

Because w is diagnostically related to Q, $\mathscr{C}$ can be expressed in a form similar to $\mathscr{H}$, as given below in (4.14). To obtain (4.14) we begin by using the relations (3.12) and (3.18) to write (4.6) as

$$\mathscr{C} = \int\int \frac{g}{\theta_0} w^*\theta\rho a\cos\Phi d\Phi dZ. \tag{4.7}$$

Using (3.6) and integrating by parts, (4.7) becomes

$$\mathscr{C} = -\int\int \psi^*\frac{g}{\theta_0}\frac{\partial\theta}{\partial\Phi}\cos\Phi d\Phi dZ. \tag{4.8}$$

Using the symbol L^* to denote the second order operator on the left-hand side of (3.7a), let us now define χ^* to be the solution of

$$L^*(\chi^*) = \frac{g}{\theta_0}\frac{\partial\theta}{a\partial\Phi}, \tag{4.9}$$

with the same homogeneous Dirichlet boundary conditions as (3.7). We can interpret χ^* as the streamfunction for a meridional displacement field in (Φ, Z) space. This field does not directly depend on the heating, but only on the instantaneous structure of the zonal wind. Substituting (4.9) into (4.8) we obtain

$$\mathscr{C} = -\int\int \psi^* L^*(\chi^*)a\cos\Phi d\Phi dZ$$

$$= -\int\int \chi^* L^*(\psi^*)a\cos\Phi d\Phi dZ. \tag{4.10}$$

The last step follows from the self-adjoint property of the linear operator L^*. Using (3.7a) in (4.10) and performing a final integration by parts, we obtain

$$\mathcal{C} = \int\int \eta^* Q \rho a \cos\Phi d\Phi dZ, \tag{4.11}$$

where

$$\rho\eta^* = \left(\frac{c_p\theta_0}{g} - Z\right)^{-1} \frac{\partial(\chi^* \cos\Phi)}{a\cos\Phi\partial\Phi}. \tag{4.12}$$

By analogy with (3.18) we define

$$\eta = \left(\frac{\zeta}{2\Omega \sin\Phi}\right)\eta^*, \tag{4.13}$$

so that (4.11) can be expressed in (ϕ, z) space as

$$\mathcal{C} = \int\int \eta Q \rho a \cos\phi d\phi dz. \tag{4.14}$$

Using (4.5) and (4.14) we can define

$$\bar{\eta} = \frac{\mathcal{C}}{\mathcal{K}} = \frac{\int\int \eta Q \rho a \cos\phi d\phi dz}{\int\int Q \rho a \cos\phi d\phi dz} \tag{4.15}$$

as the overall efficiency of the energy conversion. We shall refer to $\eta(\phi, z, t)$ as the dynamic efficiency factor and $\bar{\eta}(t)$ as the system efficiency. According to (4.15) the dynamic efficiency factor is a measure of the effectiveness of the heating at any point in producing kinetic energy. The computation of the η field at a particular instant is accomplished by solving (4.9) for χ^*, determining η^* from (4.12) and finally determining η from (4.13). Some calculations of η will be shown in section 6.

5. Solution of the meridional circulation equation for the Boussinesq, resting zonal flow case

As can be seen from the meridional circulation equation (3.7), differences between the strengths of the summer and winter Hadley cells can be related to anisotropy introduced by the variable coefficients q and s. As we shall see, variation of the coefficient s is usually the more important effect, and it is most easily illustrated in the Boussinesq, resting zonal flow case. Thus, as a first attempt to understand the difference between the summer and winter Hadley cells and the balance of terms in the thermodynamic equation, let us consider the hypothetical case in which $u = 0$ and in which ρ and $\partial\theta/\partial Z$ are constant. Under these conditions $\Phi = \phi$, $\rho A = \rho q = N^2 =$ constant, $B = 0$ and $\rho C = \rho s = 4\Omega^2 \sin^2\phi$, so that either of the meridional circulation equations (2.7) or (3.7) reduce to

$$\frac{\partial}{\partial\phi}\left(\frac{\partial(\psi\cos\phi)}{\cos\phi\,\partial\phi}\right) + \frac{4\Omega^2 a^2 \sin^2\phi}{N^2}\frac{\partial^2\psi}{\partial z^2} = \frac{\rho g a}{N^2\theta_0}\frac{\partial Q}{\partial\phi}. \tag{5.1}$$

Let us assume that Q is due to latent heat release and the horizontally varying part of the radiative forcing; the horizontally uniform part of the radiative forcing does not contribute to the right-hand side of (5.1). Specifying this heating as $Q(\phi, z) = \hat{Q}(\phi)\sin(\pi z/z_T)$, and then assuming that $\psi(\phi, z) = \hat{\psi}(\phi)\sin(\pi z/z_T)$, we obtain from (5.1) the meridional structure equation

$$\frac{d}{d\phi}\left(\frac{d(\hat{\psi}\cos\phi)}{\cos\phi d\phi}\right) - \epsilon \sin^2\phi\hat{\psi} = \frac{\rho g a}{N^2\theta_0}\frac{d\hat{Q}}{d\phi}, \tag{5.2}$$

where $\epsilon = 4\Omega^2 a^2/(gh)$ is Lamb's parameter based on the equivalent depth $h = N^2 z_T^2/(g\pi^2)$. For $z_T = 15$ km and $N = 1.2 \times 10^{-2}$ s^{-1}, we have $h = 335$ m and $\epsilon = 263$. Equation (5.2) is closely related to the differential equation for angular prolate spheroidal wave functions (Abramowitz and Stegun 1964, pages 752–769). Rather than discuss its analytical characteristics, we simply solve (5.2) numerically for the case where

$$\hat{Q}(\phi) = \hat{Q}_0 \exp[-\alpha^2(\sin\phi - \sin\phi_c)^2], \tag{5.3a}$$

with

$$\hat{Q}_0 = \left\{\frac{4\alpha}{\text{erf}[\alpha(1 + \sin\phi_c)] + \text{erf}[\alpha(1 - \sin\phi_c)]}\right\}\frac{Q_0}{\sqrt{\pi}}. \tag{5.3b}$$

Here $\hat{Q}_0$ has been chosen so that

$$\frac{1}{2}\int_{-\pi/2}^{\pi/2} \hat{Q}(\phi)\cos\phi d\phi = Q_0. \tag{5.4}$$

By varying ϕ_c and α we can now consider simulated ITCZs centered at different latitudes and with different widths. According to (5.4) these different cases will all result in the same area averaged heating Q_0. In particular, we shall set $Q_0 = 0.30$ K day^{-1}, $\alpha = 30$, 15 and $0 \leq \phi_c \leq 30$ degrees latitude. Defining the e-folding width as the latitudinal extent for which $|\sin\phi - \sin\phi_c| \leq 1/\alpha$, we see that the e-folding width of our heating is about 4 degrees latitude for $\alpha = 30$ and 8 degrees latitude for $\alpha = 15$. The choice of such narrow ITCZs is motivated by Marshall Islands rainfall data (Yanai et al. 1973, Fig. 12), by mean cloud brightness data (Miller and Feddes 1971), and by individual satellite images such as those shown in Fig. 1. The results of our solutions to (5.2) are shown in Figs. 2–4. These solutions have been obtained by discretizing (5.2) with a centered finite difference approximation, resulting in a tridiagonal matrix inversion problem. We have chosen a grid spacing of 0.01 degrees latitude, so that the discretization error in solving (5.2) is entirely negligible.

In Fig. 2 we have plotted three parameters as a function of the latitude of the peak heating—the absolute values of the maximum and minimum of $\hat{\psi}\cos\phi$ and their sum. These can be interpreted respectively as the mass flux of the summer hemisphere cell, the mass flux of the winter hemisphere cell, and the total upward mass flux in the ITCZ. Solid lines correspond to $\alpha = 30$, while dashed lines correspond to $\alpha = 15$. For the

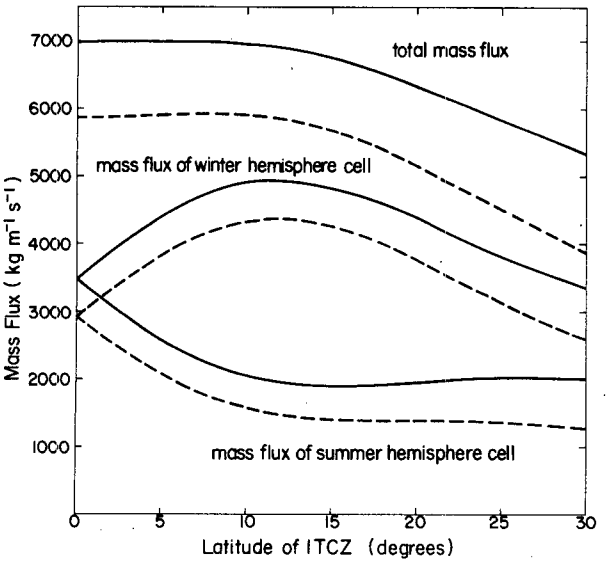

FIG. 2. Mass flux into the ITCZ from the summer hemisphere Hadley cell (lower curve), the winter hemisphere Hadley cell (middle curve), and their sum, plotted as a function of the central latitude of the ITCZ. The curves were obtained for the special case of no zonal wind by solving the meridional structure equation (5.2) with heating given by (5.3). Solid lines are for an ITCZ with an e-folding width of 4 degrees latitude ($\alpha = 30$), while dashed lines are for an e-folding width of 8 degrees latitude ($\alpha = 15$).

narrow heating ($\alpha = 30$), the maximum winter hemisphere cell mass flux occurs when the heating is centered at 12 degrees latitude while the maximum difference between the mass fluxes of the two cells occurs when the heating is centered at 13 degrees latitude. A similar response, albeit smaller in magnitude, occurs for the wide heating case.

A more complete view of the solution is shown in Figs. 3 ($\alpha = 30$) and 4 ($\alpha = 15$), in which we present the latitudinal behavior of the streamfunction $\hat{\psi}\cos\phi$, the vertical motion field w, and the potential temperature tendency $\partial\theta/\partial t$ as a function of the location of the diabatic heat source. As can be seen in Figs. 3a and 4a, when the heating is centered on the equator, two circulation cells of equal intensity are produced. As the heating is shifted off the equator, the cross-equatorial circulation cell becomes stronger while its companion cell becomes weaker. A shift in the heating poleward of 12 degrees results in a steady weakening of the winter circulation cell and more subtle changes in the summer hemisphere cell. The vertical motion fields (Figs. 3b and 4b) also exhibit asymmetry with respect to the position of the ITCZ, with a broader and significantly stronger region of subsidence on the equatorward side of the diabatic heating. The thermodynamic response (Figs. 3c and 4c) reflects this asymmetry with a much broader and enhanced warming region in the winter circulation cell. Note that despite the fact that the asymmetry of the meridional circulation cells is sensitive to the location of the diabatic heating, the thermodynamic response is relatively insensitive to its location, particularly when the peak heating lies within 6 degrees of the equator. It is also interesting to note that although the halfwidth of the heating appears to play a major role in the magnitude and structure of the meridional circulation as seen in Fig. 4, the thermodynamic response is virtually identical except in the immediate vicinity of the heating when it is located at higher latitudes. In both the $\alpha = 30$ and $\alpha = 15$ cases, the peak in the thermodynamic response is observed to be slightly poleward of the peak in the heating. The size of this displacement depends upon the halfwidth of the heating, with a broader heating producing a larger displacement. This poleward displacement effect can be seen in Fig. 4c by noting the difference in location of the peak warming ($\partial\theta/\partial t$) and the peak heating (which coincides with a line drawn from the upper left corner to the middle of the abscissa). One interpretation of these slight poleward shifts is that they are simply a manifestation of the rate at which the heating field decays with latitude as compared to the rate at which the vertical motion field decays in the same region. Such shifts are much more prominent in the solutions of Lindzen and Hou (1988) and are an essential part of their simplified balance theory of the Hadley circulation.

The nature of the meridional streamfunction response shown in Figs. 2–4 can be explained as follows. As the diabatic heating is shifted off the equator, the mass flux of the winter hemisphere cell increases because the low inertial stability in the equatorial region makes it easy to draw cross-equatorial air into the ITCZ. As the heating is shifted poleward of about 12 degrees latitude, the low inertial stability in the equatorial region is too far from the ITCZ to be effectively tapped. This notion is consistent with equatorial β-plane theory (Matsuno 1966), according to which the Rossby length scale is $\epsilon^{-1/4}a \approx 1580$ km (i.e., approximately 14 degrees latitude). In section 6 we will show how these conclusions are modified by the inclusion of a zonal flow.

6. Solution of the balanced system

We now examine the behavior of the Hadley circulation in more detail using the transformed balance model presented in (3.1)–(3.7). The details of the numerical procedures used in the solution of these equations are presented in appendix B. The experimental approach is to impose a diabatic heat source in the model atmosphere, which is initially at rest with constant static stability, and to allow the zonal flow and associated thermal field to develop over a period of a few days. Since the rate at which the zonal flow evolves depends upon the latitudinal location of the peak in the diabatic heat source, we compare all numerical results at the time at which the maximum temperature perturbation (i.e., departure from the initial state) on

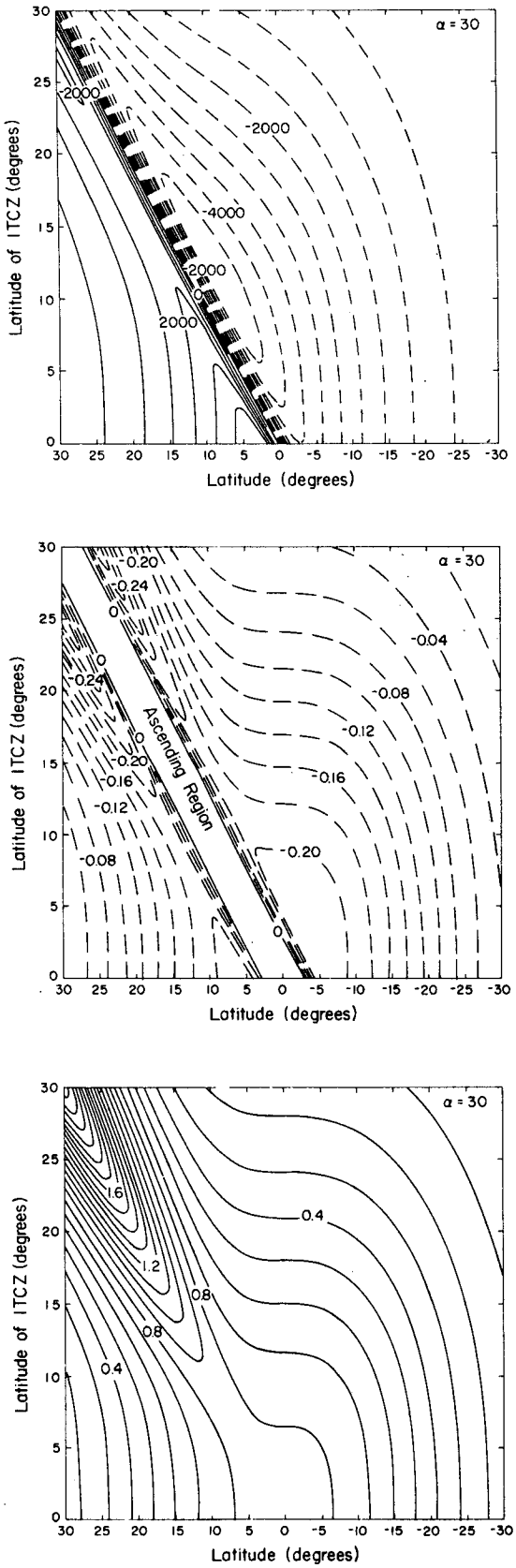

a constant z surface is slightly more than 2.5°C (an arbitrary threshold). The numerical solutions we will present produce a perturbation of this magnitude after integration times ranging from 33 hours (heating centered at 20° latitude) to 59 hours (heating centered on the equator). The diabatic forcing has the same horizontal physical space structure given in (5.3), and a vertical structure corresponding to the apparent heat source obtained by Yanai et al. (1973, Fig. 10) in their analysis of Marshall Islands data. For the following experiments, we have normalized the amplitude of the Yanai heating profile so that it produces a globally averaged heating rate of 0.30°C/day at its peak value in the vertical (i.e., near 500 mb).

Figure 5 illustrates the dependence of the meridional circulation on the location of the diabatic heating. In analogy with Fig. 3, we have plotted the absolute values of the maximum and minimum of $\psi \cos\phi$, and their sum as a function of the latitude of the diabatic forcing. In addition to the resting state values for these parameters (solid lines), we have also plotted them for the zonal flows that have developed by the end of the numerical integration (dashed lines). The qualitative behavior of these quantities is quite similar to the more idealized results presented in section 5. In slight contrast with the Boussinesq solutions, the balanced model integrations show that both the maximum winter hemisphere cell mass flux and maximum asymmetry occur when the heating is centered somewhat closer to the equator, or at 10 degrees and 12 degrees latitude respectively. The spinup of the zonal flow makes relatively minor modifications to the meridional mass flux parameters, introducing maximum departures on the order of 5% when the peak in the heating is located in the equatorial region. These small modifications to the mass flux parameters, arising from the developing zonal flow, cause the largest winter hemisphere mass flux to be associated with an ITCZ position of 13 degrees latitude.

The structure of the meridional and zonal circulations that develop in response to several selected locations of the diabatic heat source are shown in Fig. 6. The figure includes the meridional streamfunction $\psi a \cos\phi$, the zonal wind u, the departure of the temperature field from the initial state, and the efficiency parameter η, given by (4.13), for heating centered at 0, 5, 10, and 20 degrees latitude. The generation of a 2.5°C temperature perturbation produces zonal flows with maximum amplitudes between 4 and 7 m s^{-1} in all cases, although the jet structures differ sharply for particular meridional locations of the diabatic forcing. As suggested by Fig. 5, the largest asymmetries in the meridional circulation occur when the peak in the dia-

FIG. 3. The meridional structure of the streamfunction $\psi \cos\phi$ (kg m^{-1} s^{-1}), vertical motion w (contour interval of 0.02 cm s^{-1}), and thermodynamic response $\partial\theta/\partial t$ (contour interval of 0.1° day^{-1}) as a function of the central latitude of the ITCZ for $\alpha = 30$.

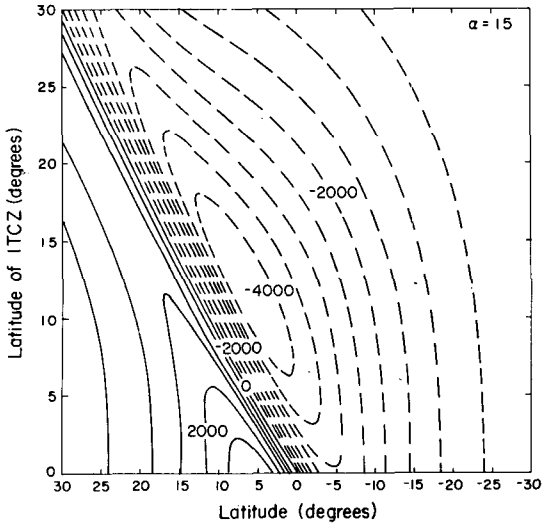

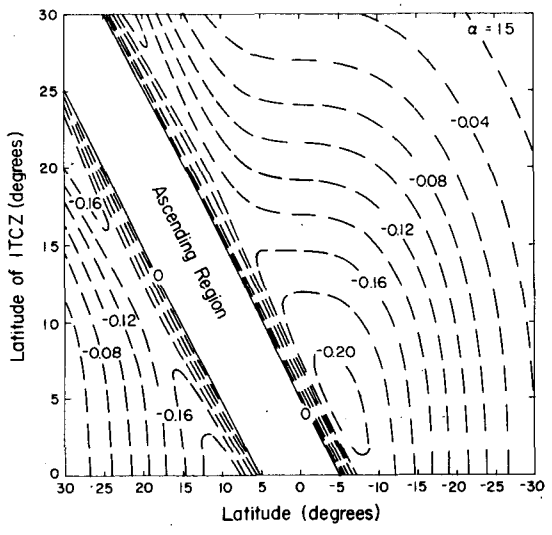

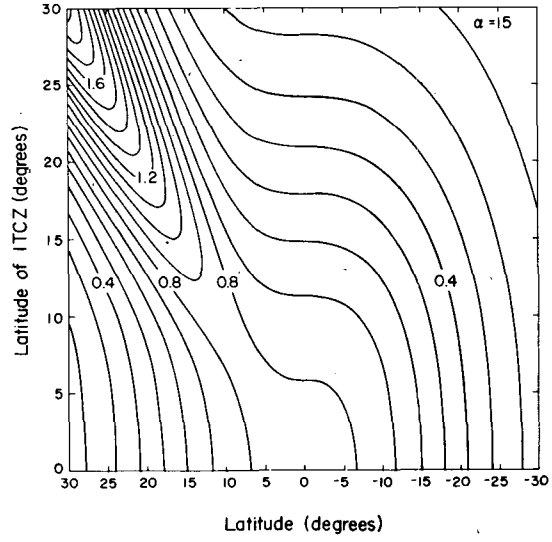

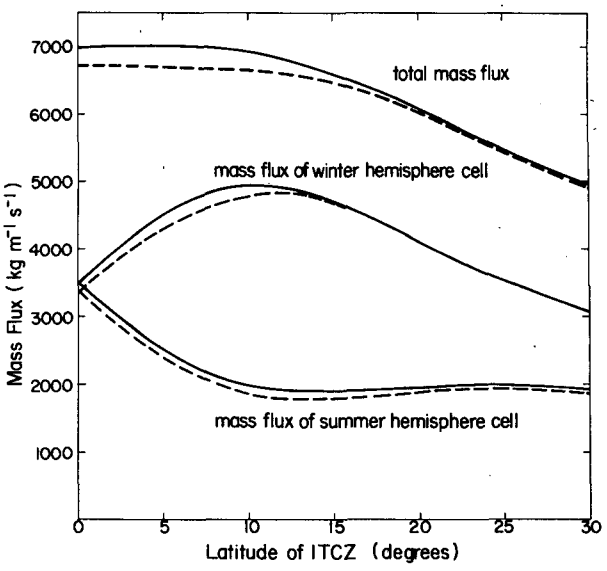

FIG. 5. Mass flux into the ITCZ from the summer hemisphere Hadley cell (lower curves), the winter hemisphere Hadley cell (middle curves), and their sum, plotted as a function of the central latitude of the ITCZ. The curves were obtained by solving the meridional structure equation (3.7) with meridional heating structure given by (5.3) for which $\alpha = 30$, and vertical structure given by Yanai et al. (1973). Solid curves are for the initial time when the zonal flow vanishes, while dashed lines are for a basic state flow that evolves in response to the heating and that exhibits a 2.5°C temperature perturbation.

batic heating is within 15 degrees of the equator. It is interesting to compare the case where the peak heating is centered on the equator with the case where it is centered at 5 degrees latitude. As suggested by the Boussinesq results, although a large asymmetry in $\psi a \cos\phi$ exists when the heating is centered at 5 degrees latitude (both with respect to the diabatic heat source and the equator), it is not strongly reflected in either the temperature or η fields, which differ only slightly from their $\phi_c = 0$ counterparts.

As the peak forcing is moved poleward of 10 degrees latitude, significant changes appear in the structure and scale of the thermodynamic response, the most important of which is the asymmetric character of this field with respect to the diabatic heat source. The thermodynamic field responds in a broad but very asymmetric way with respect to the location of the ITCZ as it moves away from the equator, followed by a highly localized and more symmetric response poleward of 20 degrees latitude. The dramatic reduction in the horizontal extent of the thermodynamic response can be seen by examining the 1°C perturbation contour, which extends over 45 degrees of latitude when the peak heat-

FIG. 4. The meridional structure of the streamfunction $\psi \cos\phi$ (kg m^{-1} s^{-1}), vertical motion w (contour interval of 0.02 cm s^{-1}), and thermodynamic response $\partial\theta/\partial t$ (contour interval of 0.1° day^{-1}) as a function of the central latitude of the ITCZ for $\alpha = 15$.

ing is equatorward of 10 degrees latitude and over only 17 degrees of latitude when the heating is centered at 20 degrees latitude (e.g., the Indian monsoon). Of equal interest is the asymmetric nature of the thermal response with respect to the ITCZ, which becomes most pronounced when the peak in the diabatic heating is located near 10 degrees latitude. For example, when the heating is centered at 10 degrees latitude, a 2°C response can be seen 6 degrees poleward of the heating in the summer hemisphere, but 18 degrees poleward in the winter hemisphere. This behavior, which is qualitatively present in all cases, implies that even though the horizontal scale of the winter hemisphere circulation cell appears to be considerably broader than the horizontal scale of the summer cell, the subsidence produced in the descending branch of the winter cell is significantly larger. This behavior was also suggested by the Boussinesq solutions presented in section 5. A direct consequence of such an asymmetry might be a lower trade wind inversion height equatorward of the ITCZ.

Finally, the bottom panels in Fig. 6 show the changes in the structure and magnitude of the dynamic efficiency parameter η as the location of the ITCZ is moved away from the equator. As mentioned earlier, the meridional structure of η exhibits only minor changes when the heating is located within 5 degrees of the equator. The magnitude of this quantity is also fairly insensitive to the location of the heating equatorward of 10 degrees, where the peak value increases by less than 25% as the diabatic heating is moved from the equator to 10 degrees latitude. An even smaller growth of 13% in the system efficiency, $\bar{\eta}$, which is a measure of the overall kinetic energy generation rate, is seen for displacement of the diabatic heat source in the same region. As the diabatic forcing moves poleward of 10 degrees latitude, however, a rapid increase in the magnitude of η is observed, with the peak value increasing by more than 60% for a heat source located at 20 degrees latitude. The η field also exhibits a contraction in horizontal scale similar to what is observed in the thermodynamic field, the gradient of which appears on the right-hand side of Eq. (4.9) (from which η is determined). This contraction in horizontal scale is the primary reason why a comparable increase in $\bar{\eta}$ accompanies the large growth in the peak value of η as the ITCZ moves poleward of 10 degrees latitude.

The rapid increase in η and $\bar{\eta}$ as our model ITCZ is moved poleward of 10 degrees latitude is consistent with observational studies which show explosive growth in the rate of kinetic energy generation as the atmosphere's ITCZ migrates poleward of this latitude (e.g., Krishnamurti et al. 1981; Krishnamurti and Ramanathan 1982). We note that for a fixed location of the ITCZ heating, the time rate of change in the structure and magnitude of the efficiency field are primarily determined by the properties of the temperature and normalized potential vorticity fields, since the inertial stability field is only slightly modified by the developing zonal flow. Our numerical integrations show that the structures of q, θ, and η in the meridional plane are relatively invariant in time (for a fixed ITCZ location), while the magnitude of the q field grows exponentially, and the magnitudes of the θ and η fields grow linearly. This contrasts sharply with the physical mechanisms related to hurricane development, where the development of the s field plays a fundamental role in the nonlinear time dependent evolution of η (see Hack and Schubert 1986). One characteristic these two phenomena do share is that relatively small horizontal displacements of the heating produce large differences in the rate of kinetic energy generation. Thus, as the ITCZ shifts its location away from the equator, the rate at which balanced zonal flow is generated increases, particularly poleward of 10 degrees latitude.

Typical examples of s and q are shown in Fig. 7 for the case where the heating is centered at 10 degrees latitude. Note that the zonal flow has produced relatively small modifications to the inertial stability parameter, but it has resulted in a normalized potential vorticity field that varies from its resting state value by more than a factor of 4. Increased q at low levels and decreased q at high levels is the fundamental atmospheric response to convective forcing and has recently been discussed in the contexts of tropical cyclones (Schubert and Alworth 1987) and squall lines (Schubert et al. 1989). The quantity $(s/q)^{1/2}$, shown in the last panel of Fig. 7, is proportional to the inverse of the generalized Rossby radius of deformation, and exhibits large changes in the vicinity of the diabatic heat source. These changes suggest an increase in the local Rossby radius at low levels, with a sharp decrease in this parameter in the upper levels. This result is quite different from the hurricane case, once again due to the lack of a significant modification of the inertial stability field.

Although the inertial stability may not appear to play a large role in the time dependent characteristics of the efficiency field, it probably does play an important role in determining the meridional structure of η since, as the heating is moved poleward, the fluid becomes stiffer to meridional displacements in response to increasing s, resulting in increasingly larger peak values of η, as well as a focusing of the response. The increase in the peak value of η appears to flatten out poleward of 20 degrees due to a slower decay in the local magnitude of the potential vorticity, as compared to the rate at which the inertial stability is increasing in the same region.

7. Concluding remarks

In this paper we have used the balance system of equations to examine the response of the mean meridional circulation to diabatic heating produced by cumulus convection in the ITCZ. Solving both a simplified meridional circulation equation, in which $u = 0$

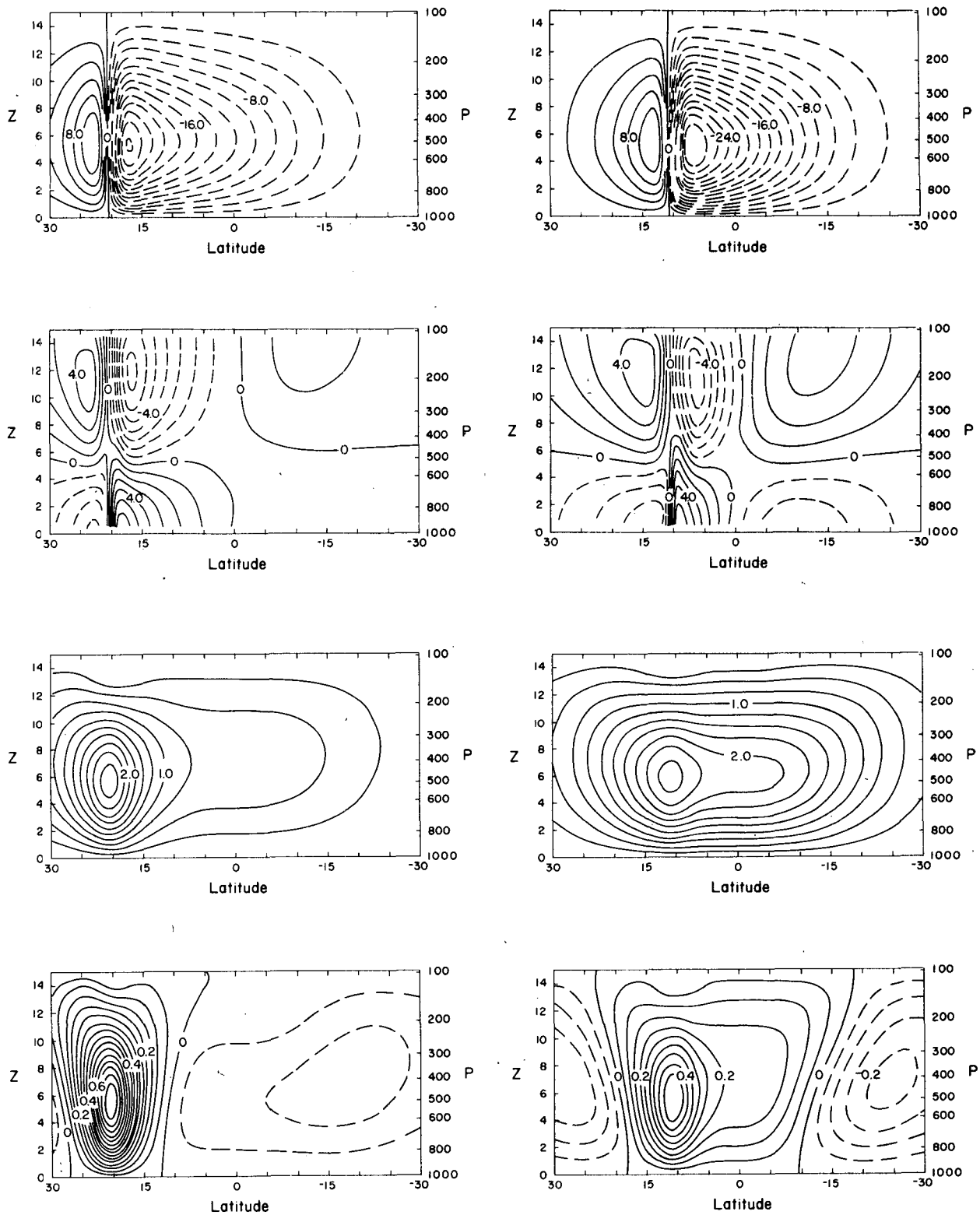

FIG. 6. Each vertical column of four panels shows the meridional circulation $a\psi\cos\phi$ (2×10^9 kg s^{-1} rad^{-1} contour interval), the zonal wind u (0.5 m s^{-1} contour interval), temperature perturbation (0.25°C contour interval) and the dynamic efficiency factor η (0.05% contour interval). Vertical columns are for heating centered at (a) 20°N, (b) 10°N, (c) 5°N, and (d) 0°N.

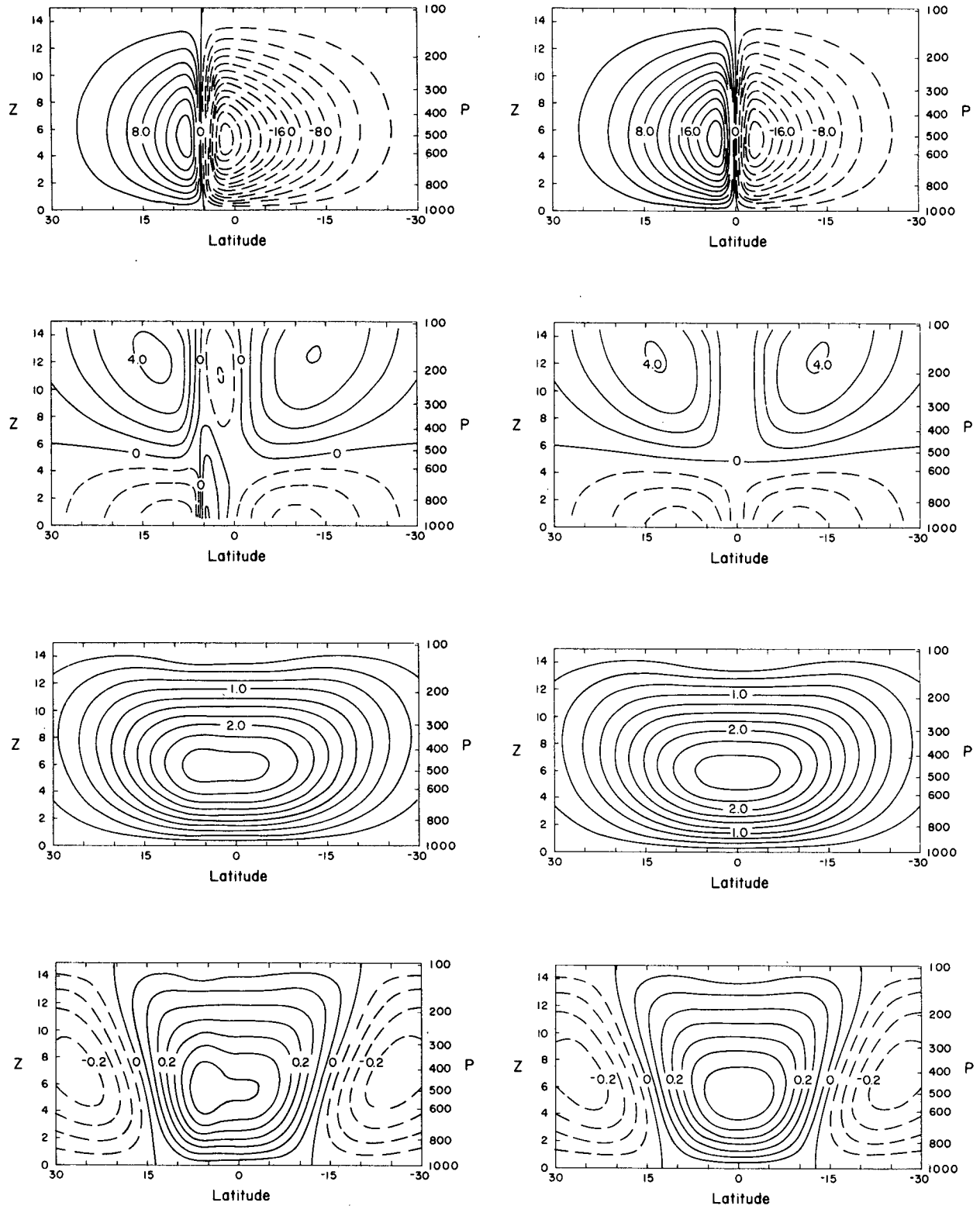

FIG. 6. (*Continued*)

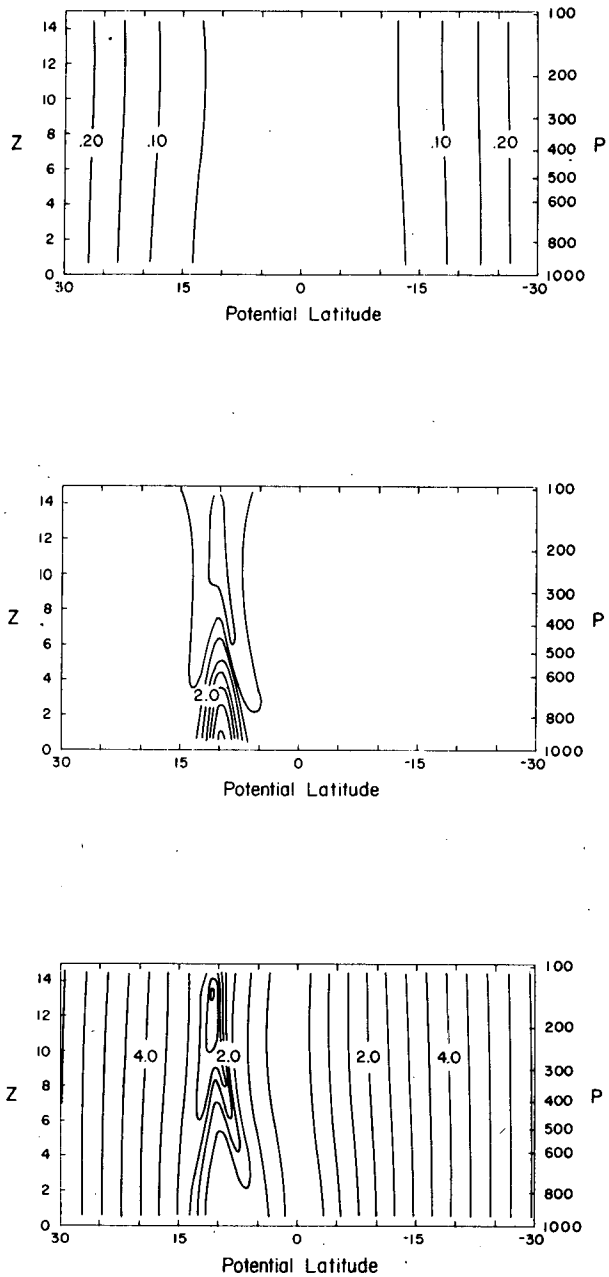

FIG. 7. Typical example of the spatial distribution of the coefficients which appear in the meridional circulation equation (3.7). The top panel shows ρs normalized by $4\Omega^2$ (0.05 contour interval), the middle panel shows ρq normalized by its initial value N^2 (0.5 contour interval), and the bottom panel shows $(s/q)^{1/2}$ (0.5×10^{-3} contour interval), which is proportional to the inverse of the generalized Rossby radius. In the special case where $\psi^*(\Phi, Z) = \Psi^*(\Phi)\sin(\pi Z/Z_T)$ and $Q(\Phi, Z) = \hat{Q}(\Phi)\sin(\pi Z/Z_T)$ the quantity $(Z_T/\pi)(q/s)^{1/2}$ can be thought of as the generalized Rossby radius. All panels are given in (Φ, Z) space for an ITCZ centered at 10°N and for the zonal flow shown in Fig. 6c.

and the vertical variation of the pseudo-density is neglected, and the more general transformed balance system, illustrates a rapid change in the difference between the winter and summer circulation cells that accompanies the movement of the diabatic heat source off of the equator. This difference reaches a maximum when the diabatic heating is centered 12 degrees from the equator; at this point the strength of the winter circulation cell is more than twice that of the summer circulation cell. Our solutions also show that even if the integrated heating is held fixed, the halfwidth of the heating plays a major role in determining the magnitude and structure of the meridional circulation. The presence of the zonal flow that develops in response to the specified diabatic heat source makes only minor modifications to the solutions.

The differences in the two meridional circulation cells are reflected in the magnitude and breadth of the vertical motion fields occurring in the descending branch of each cell. Significantly stronger and broader subsidence is produced on the equatorward side of the diabatic heating when it is located within 10 degrees of the equator. It may be of interest to consider the effects that these differences may have on the trade wind boundary layer. The large-scale subsidence rate is generally accepted as the major control on the depth of the trade wind boundary layer. Thus, at a given distance away from the ITCZ on the winter hemisphere side we might expect a shallower boundary layer than that which exists at the same distance away from the ITCZ on the summer hemisphere side. For example, compare the region between 20°N and 25°N to the region between the equator and 5°S for the case when the ITCZ is centered at 10°N. As can be seen in the streamfunction diagram in Fig. 6, the subsidence rate is about twice as strong on the winter hemisphere side. This is also reflected in the θ field, which shows a temperature perturbation about twice as strong on the winter hemisphere side. Thus, if other effects such as sea surface temperature remain of secondary importance, we might expect a trade wind boundary layer considerably shallower on the winter hemisphere side. Some observational evidence in support of this argument can be found in the work of Ramage et al. (1981), who analyzed aircraft data from six NOAA P-3 shuttle flights southward from Hawaii to Tahiti along 150°W and the six return flights northward from Tahiti to Hawaii along 158°W. These flights were made between 29 November 1977 and 5 January 1978 when the average ITCZ position was 7°N. Ramage et al. report that the median height of the base of dry air just above the trade inversion was about 1950 m in the region 7.5 degrees north of the ITCZ and 1390 m in the region 7.5 degrees south of the ITCZ. If the moist layer on the winter side of the ITCZ is really shallower, we have a situation where the air in the shallow moist layer on the winter side is flowing toward the ITCZ faster than the air in the deep moist layer on the summer side. This would tend to make the difference in the moisture flux toward the ITCZ considerably less than the difference in the mass flux.

Although the structure of the meridional circulation is quite sensitive to the location and horizontal scale of the diabatic heat source when it is located within 10 degrees latitude of the equator, the tropical thermodynamic response exhibits virtually no sensitivity, particularly when the heating is located equatorward of 6 degrees latitude. Except in the immediate vicinity of the heating, the thermodynamic structure is also relatively insensitive to the horizontal scale of the diabatic heat source.

Finally, we have shown how the efficiency of latent heat release at generating balanced zonal flow depends on the zonal flow itself. In the Northern Hemisphere, when the lower troposphere has stronger easterlies north of the ITCZ and stronger westerlies south of the ITCZ, the efficiency of latent heat release generally tends to be higher. The magnitude of the zonal circulation is of most importance to the generation of kinetic energy when the ITCZ is located equatorward of 10 degrees latitude. Poleward of 10 degrees latitude, small meridional displacements of the ITCZ can be of comparable importance to increases in the local magnitude of the zonal circulation, as far as the efficiency of latent heat release is concerned.

It is well known that a necessary condition for instability of the zonal flow is a reversal of the meridional gradient of potential vorticity on isentropic surfaces (Charney and Stern 1962; Eliassen 1983), i.e., $(\partial P/\partial\phi)_\theta < 0$. For example, the origin of easterly waves in the Atlantic has been linked to observed reversals in the gradient of potential vorticity that occur downstream of the Abyssinian mountains on the African continent, where the lower easterly current first becomes organized and exhibits a sharp meridional thermal contrast for many hundreds of kilometers (e.g., Burpee 1972; Reed et al. 1977). As discussed in section 6, our numerical results show that a fundamental atmospheric response to latent heat released in deep cumulus convection is the generation of increased potential vorticity at low levels and decreased potential vorticity at high levels. This response has particular significance with respect to the ITCZ and the formation of easterly waves, as can be seen in Fig. 8, a snapshot of the Rossby–Ertel potential vorticity P for the case where the specified diabatic heat source is located at 10 degrees north. The shading denotes regions where the meridional gradient of potential vorticity on isentropic surfaces reverses. Note that the region of reversed P gradient is poleward of the ITCZ in the lower troposphere and equatorward of the ITCZ in the upper troposphere. With normal ITCZ convection and rainfall, the time scale for producing such potential vorticity gradient reversals is quite short—on the order of a day or two. Thus, such gradient reversals are probably not confined to just the African wave generation region, but may also play an important role in ITCZ breakdown in other regions such as the eastern Pacific region shown in Fig. 1. In this sense the ITCZ contains the seeds of its own destruction, and it can be regarded as a highly dynamic phenomenon that tends to form, break down and reform on the time scale of weeks. If tropical easterly waves are generated in the unstable lower tropospheric region poleward of the ITCZ, and if these waves continue to develop into tropical cyclones, we might expect the east–west line of ITCZ convection to be deformed by the rotational motion of the cyclone. Thus, at least some spiral features of tropical cyclones, such as those shown in Fig. 1b, may simply be the lower tropospheric high potential vorticity remnants of the ITCZ.

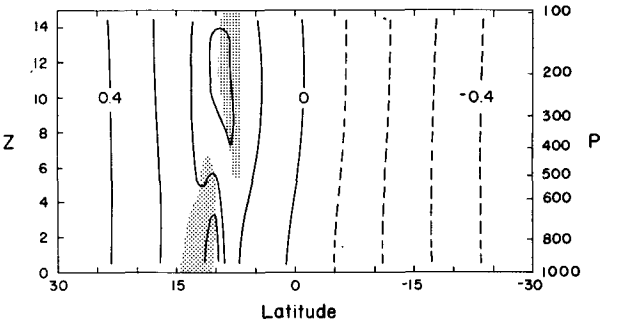

FIG. 8. Meridional cross section of the Rossby–Ertel potential vorticity P, normalized by $2\Omega N^2\theta_0/(g\rho)$, which is the value of P at the North Pole in a resting atmosphere. This potential vorticity field results from 30 hours of model integration using the heating field (5.3) with an ITCZ position $\phi_c = 10°$N and $\alpha = 30$. The stippled areas indicate where $(\partial P/\partial\phi)_\theta < 0$. The region between the $P = 0$ and $\phi = 0$ lines has $P\sin\phi < 0$ and is hence slightly nonelliptic.

Acknowledgments. We wish to thank Paul Ciesielski, T. N. Krishnamurti and Bruce Albrecht for their helpful comments, Jenny Martin for her help in the preparation of the manuscript, and Suzanne Whitman for drafting the figures. This research was also supported by NSF Grants ATM 8510664, ATM 8609731 and ATM 8814541.

APPENDIX A

Derivation of the Transformed Balance, Zonal Momentum and Continuity Equations

To transform the balance equation (2.1) into (3.1), we first note that (2.1) can be written as

$$\zeta u + \frac{\partial G^*}{a\partial\phi} = 0. \tag{A.1}$$

Applying (3.10) to G^*, substituting the result into (A.1), and then using (3.12), we can write the balance relation as

$$2\Omega\sin\Phi\frac{\cos\Phi}{\cos\phi}u + \frac{\partial G^*}{a\partial\Phi} = 0. \tag{A.2}$$

The form (3.1) follows directly from (A.2). In addition, the elimination of u between (2.1) and (A.2) leads to the relation (3.22).

To derive the zonal momentum equation (3.2) from (2.2) we first note that (2.2) can be written

$$\frac{\partial u}{\partial t} + w\frac{\partial u}{\partial z} - \zeta v = 0, \tag{A.3}$$

and that application of (3.9) and (3.11), with the use of (3.8) and (3.20), leads to

$$2\Omega \sin\phi \frac{\partial(u\cos\phi)}{\partial t} = \zeta \frac{\partial(u^*\cos\Phi)}{\partial T}, \tag{A.4}$$

$$2\Omega \sin\phi \frac{\partial(u\cos\phi)}{\partial z} = \zeta \frac{\partial(u^*\cos\Phi)}{\partial Z}. \tag{A.5}$$

Multiplication of (A.3) by $\cos\phi$ followed by the use of (A.4), (A.5) and (3.17) leads directly to the transformed zonal momentum equation (3.2).

The transformed continuity equation can be derived from first principles (see Shutts 1980) or, as we shall do here, from the vertical component of the vector vorticity equation (2.8), which can be written

$$\frac{D\zeta}{Dt} - \frac{\partial u}{\partial z}\frac{\partial w}{a\partial\phi} + \zeta\frac{\partial(v\cos\phi)}{a\cos\phi\partial\phi} = 0, \tag{A.6}$$

where ζ is given by the second component in (2.10). Using the continuity equation (2.4), the derivative relations (3.10) and (3.11), and the definition (3.8), we can write (A.6) as

$$\frac{D\zeta}{Dt} - \zeta\frac{\partial(\rho w)}{\rho\partial Z} = 0. \tag{A.7}$$

Using (3.15) we can write (A.7) in the flux form

$$\frac{\partial}{\partial T}\left(\frac{2\Omega\ \sin\Phi}{\zeta}\right) + \frac{\partial}{\rho\partial Z}\left(\frac{2\Omega\sin\Phi}{\zeta}\rho w\right) = 0. \tag{A.8}$$

Using (3.20) to express $2\Omega\sin\Phi/\zeta$ in terms of u^* and (3.2) to express $\partial u^*/\partial T$ in terms of v^*, we find that (A.8) reduces to the transformed continuity equation (3.4).

APPENDIX B

Numerical Methods

The numerical integration of the transformed balance system shown in the right side of Table 1 is performed using a finite difference procedure as follows. The horizontal domain is partitioned into I equal intervals separated by the $I+1$ points $\Phi_i = -\pi/2 + i\Delta\Phi$ ($i = 0, 1, 2, \cdots, I$), while the vertical domain is divided into J equal intervals separated by the $J+1$ points $Z_j = j\Delta Z$ ($j = 0, 1, 2, \cdots, J$). Staggered midway between the Φ_i and Z_j points are the points $\Phi_{i+(1/2)}$ and $Z_{j+1/2}$. The distribution of the variables over these points is shown in Fig. 9. The south and north poles are columns along which ϕ, v^* and ψ^* are defined, while the lower and upper boundaries are levels where θ, w^*, and ψ^* are defined. For the numerical solutions presented in section 6 we have chosen $I = 360$, $J = 15$, $\Delta\Phi = 0.5°$ and $\Delta Z = 1$ km.

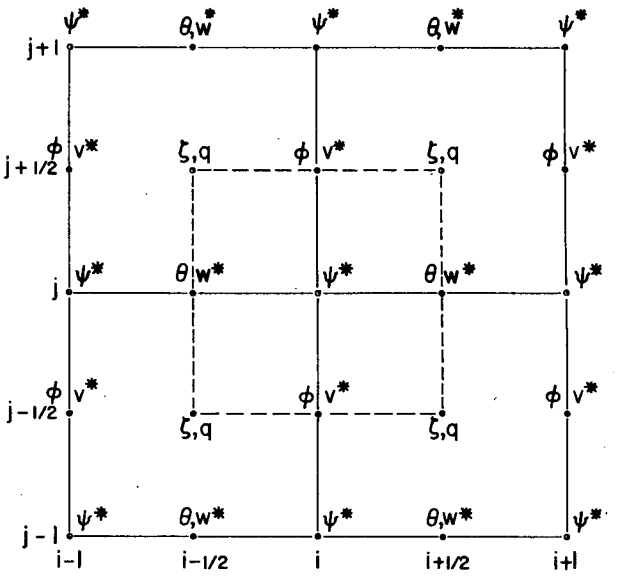

FIG. 9. Finite difference grid used for solution of the transformed balance system of equations.

The solution procedure begins by evaluating the θ field from the time dependent variable ϕ using the thermal wind equation in the form

$$2\Omega\sin\Phi\frac{\partial}{\partial Z}\left(\frac{\Omega a\cos^3\Phi}{\cos^2\phi}\right) + \frac{g}{\theta_0}\frac{\partial\theta}{a\partial\Phi} = 0, \tag{B.1}$$

followed by the diagnosis of normalized potential vorticity q and inertial stability s using (3.7b) and (3.7c), the solution of the meridional circulation equation (3.7a), the diagnosis of the meridional circulation component v^* using (3.6), and finally the prediction of a new ϕ field using

$$\frac{\partial\phi}{\partial T} = \frac{v^*\cos\Phi}{a\cos\phi}. \tag{B.2}$$

In discrete form, (B.1) is written as

$$\theta_{i+1/2,j} = \theta_{i-1/2,j} - \frac{\theta_0\Omega a^2\Delta\Phi}{g\Delta Z}2\Omega\sin\Phi_i \times\left(\frac{\cos^3\Phi_i}{\cos^2\phi_{i,j+1/2}} - \frac{\cos^3\Phi_i}{\cos^2\phi_{i,j-1/2}}\right). \tag{B.3}$$

The discrete representation of the transverse circulation equation can be written

$$\alpha_{i-1/2,j}\cos\Phi_{i-1}\psi^*_{i-1,j} + \alpha_{i+1/2,j}\cos\Phi_{i+1}\psi^*_{i+1,j} + s_{i,j+1/2}\psi^*_{i,j+1} + s_{i,j-1/2}\psi^*_{i,j-1} - \{\cos\Phi_i[\alpha_{i-1/2,j} + \alpha_{i+1/2,j}] + s_{i,j+1/2} + s_{i,j-1/2}\}\psi^*_{i,j} = \frac{g(\Delta Z)^2}{\theta_0}\left(\frac{\partial Q}{a\partial\Phi}\right)_{i,j}, \tag{B.4}$$

where

$$\alpha_{i-1/2,j} = \left(\frac{\Delta Z}{a\Delta\Phi}\right)^2 \frac{q_{i-1/2,j+1/2} + q_{i-1/2,j-1/2}}{2\cos\Phi_{i-1/2}}, \tag{B.5}$$

$$(\rho q)_{i+1/2,j+1/2} = \left(\frac{\sin\Phi_i - \sin\Phi_{i+1}}{\sin\phi_{i,j+1/2} - \sin\phi_{i+1,j+1/2}}\right) \times \frac{g}{\theta_0}\left(\frac{\theta_{i+1/2,j+1} - \theta_{i+1/2,j}}{\Delta Z}\right), \tag{B.6}$$

$$(\rho s)_{i,j+1/2} = 4\Omega^2 \sin\phi_{i,j+1/2} \sin\Phi_i \frac{\cos^3\Phi_i}{\cos^3\phi_{i,j+1/2}}. \tag{B.7}$$

Finally, the discrete form of (B.2) is given by

$$\phi^{n+1}_{i,j+1/2} = \phi^{n-1}_{i,j+1/2} + \frac{2\Delta T v^*_{i,j+1/2}\cos\Phi_i}{a\cos\phi^n_{i,j+1/2}}, \tag{B.8}$$

where

$$v^*_{i,j+1/2} = \frac{\psi^*_{i,j} - \psi^*_{i,j+1}}{\rho_{j+1/2}\Delta Z}. \tag{B.9}$$

The solution of (B.4) is accomplished with a red–black successive overrelaxation procedure. For the resolution previously described, convergence is generally obtained with less than 100 iterations.

REFERENCES

Abramowitz, M., and I. Stegun, 1964: *Handbook of Mathematical Functions.* Dover, 1046 pp.

Burpee, R. W., 1972: The origin and structure of easterly waves in the lower troposphere of North Africa. *J. Atmos. Sci.*, **29,** 77–90.

Charney, J. G., and M. E. Stern, 1962: On the stability of internal baroclinic jets in a rotating atmosphere. *J. Atmos. Sci.*, **19,** 159–172.

Eliassen, A., 1983: The Charney–Stern theorem on barotropic-baroclinic instability. *Pure Appl. Geophys.*, **121,** 563–572.

Gill, A. E., 1982: *Atmosphere–Ocean Dynamics.* Academic Press, 662 pp.

Hack, J. J., and W. H. Schubert, 1986: Nonlinear response of atmospheric vortices to heating by organized cumulus convection. *J. Atmos. Sci.*, **43,** 1559–1573.

Held, I. M., and A. Y. Hou, 1980: Nonlinear axially symmetric circulations in a nearly inviscid atmosphere. *J. Atmos. Sci.*, **37,** 515–533.

Hoskins, B. J., 1975: The geostrophic momentum approximation and the semi-geostrophic equations. *J. Atmos. Sci.*, **32,** 233–242.

——, and F. P. Bretherton, 1972: Atmospheric frontogenesis models: mathematical formulation and solution. *J. Atmos. Sci.*, **29,** 11–37.

Krishnamurti, T. N., and Y. Ramanathan, 1982: Sensitivity of the monsoon onset to differential heating. *J. Atmos. Sci.*, **39,** 1290–1306.

——, P. Ardanuy, Y. Ramanathan and R. Pasch, 1981: On the onset vortex of the summer monsoons. *Mon. Wea. Rev.*, **109,** 344–363.

Lindzen, R. S., and A. Y. Hou, 1988: Hadley circulations for zonally averaged heating centered off the equator. *J. Atmos. Sci.*, **45,** 2416–2427.

Matsuno, T., 1966: Quasi-geostrophic motions in the equatorial area. *J. Meteor. Soc. Japan,* **44,** 25–43.

Miller, D. B., and R. G. Feddes, 1971: Global atlas of relative cloud cover 1967–1970. Joint production by U.S. Department of Commerce and U.S. Air Force, Washington D.C. [Available from NTIS, Springfield, Va., AD739 434.]

Newell, R. E., J. W. Kidson, D. G. Vincent and G. J. Boer, 1972: *The General Circulation of the Tropical Atmosphere and Interactions with Extratropical Latitudes,* Vol. I. MIT Press, 258 pp.

Oort, A. H., 1983: Global Atmospheric Circulation Statistics 1958–1973. NOAA Professional Paper 14, U.S. Government Printing Office, 180 pp.

Ramage, C. S., S. J. S. Khalsa and B. N. Meisner, 1981: The central Pacific near-equatorial convergence zone. *J. Geophys. Res.*, **86,** 6580–6598.

Reed, R. J., D. C. Norquist and E. E. Recker, 1977: The structure and properties of African wave disturbances as observed during Phase III of GATE. *Mon. Wea. Rev.*, **105,** 317–333.

Schneider, E. K., 1977: Axially symmetric steady state models of the basic state for instability and climate studies. Part II: Nonlinear calculations. *J. Atmos. Sci.*, **34,** 280–296.

Schubert, W. H., 1985: Semigeostrophic theory. *J. Atmos. Sci.*, **42,** 1770–1772.

—— and J. J. Hack, 1983: Transformed Eliassen balanced vortex model. *J. Atmos. Sci.*, **40,** 1571–1583.

——, and B. T. Alworth, 1987: Evolution of potential vorticity in tropical cyclones. *Quart. J. Roy. Meteor. Soc.*, **113,** 147–162.

——, S. R. Fulton and R. F. A. Hertenstein, 1989: Balanced atmospheric response to squall lines. *J. Atmos. Sci.*, **46,** in press.

Shutts, G. J., 1980: Angular momentum coordinates and their use in zonal, geostrophic motion on a hemisphere. *J. Atmos. Sci.*, **37,** 1126–1132.

Stevens, D. E., 1983: On symmetric stability and instability of zonal mean flows near the equator. *J. Atmos. Sci.*, **40,** 882–893.

Yanai, M., S. Esbensen and J.-H. Chu, 1973: Determination of bulk properties of tropical cloud clusters from large-scale heat and moisture budgets. *J. Atmos. Sci.*, **30,** 611–627.